PNAS
www.pnas.org

Supplementary Information for

Kristian K. Kristensen[1,2,*], Katrine Zinck Leth-Espensen[1,2,3,*], Haydyn D.T. Mertens[4], Gabriel Birrane[5], Muthuraman Meiyappan[6], Gunilla Olivecrona[7], Thomas J.D. Jørgensen[3], Stephen G. Young[8,9], and Michael Ploug[1,2,‡]

From the [1]Finsen Laboratory, Rigshospitalet, DK–2200 Copenhagen N, Denmark; [2]Biotech Research and Innovation Centre (BRIC), University of Copenhagen, DK-2200 Copenhagen N, Denmark; [3]Department of Biochemistry and Molecular Biology, University of Southern Denmark, DK–5320 Odense M, Denmark; [4]European Molecular Biology Laboratory Hamburg, Notkestrasse 85, D-22607 Hamburg, Germany; [5]Division of Experimental Medicine, Beth Israel Deaconess Medical Center, Boston, MA 02215; [6]Discovery Therapeutics, Takeda Pharmaceutical Company Ltd., Cambridge, MA 02142; [7]Department of Medical Biosciences,[*] Umeå University, Umeå, Sweden; [8]Department of Medicine, University of California, Los Angeles, CA 90095; [9]Department of Human Genetics, University of California, Los Angeles, CA 90095

Stephen G. Young and Michael Ploug
Email: sgyoung@mednet.ucla.edu and m-ploug@finsenlab.dk

This PDF file includes:

www.pnas.org/cgi/doi/10.1073/pnas.1920202117

Supplementary Information Text

Materials and Methods

Surface plasmon resonance. To define the functional epitope on LPL for the monoclonal antibody 5D2, we determined the binding kinetics for the interactions between immobilized 5D2 and LPL's C-terminal domain (CTD) as well as representative synthetic peptides with surface plasmon resonance (SPR) on a Biacore T200™ system (GE Healthcare). To this end, we first immobilized the monoclonal mouse anti-LPL antibody 5D2 (1) directly on a CM5 sensor chip using *N*-hydroxysuccinimide and *N*-ethyl-*N*-(3-(diethylamino)propyl)-carbodiimide as coupling chemistry. With 5 µg 5D2/ml in 10 mM sodium acetate, pH 5.0, we obtained a surface density of 2300 resonance units (RU), which corresponds to 15.3 fmols 5D2 mAb/mm^2 (assuming one RU ~ 1 pg/mm^2). Injecting 1 M ethanolamine inactivated excess NHS-esters. Kinetic rate constants for the various analytes were determined using single cycle protocols where five serial 2-fold dilutions of the interaction partner were injected for 200 s without intervening regeneration and followed by a longer dissociation phase after the last injection (2,500 to 30,000 s dependent on the dissociation rate constant k_{off}). Interactions were measured at 40 µl/min in 10 mM HEPES, 150 mM NaCl, 3 mM EDTA, and 0.05% (v/v) surfactant P-20 at pH 7.4 at 20°C. Two consecutive injections with 10 µl of 20 mM H_3PO_4 at the end of each single cycle regenerated the chip.

With the BiacoreT200 Evaluation™ 3.0 software (supplied with the instrument), we globally fitted the double blank-referenced data by non-linear regression to a simple bimolecular interaction model. Assuming pseudo-first order reaction conditions, we derived the association (k_{on}) and dissociation (k_{off}) rate constants, the K_D (k_{off}/k_{on}), as well as the binding capacity (R_{max}).

Small-angle X-ray scattering (SEC-SAXS). Synchrotron radiation X-ray scattering data coupled to an in-line chromatography system (SEC-SAXS) were collected on the EMBL P12 beamline of the storage ring PETRA III (DESY, Hamburg) (Table S1) (2), using PILATUS 6M and 2M pixel detectors (DECTRIS, Switzerland). 50-200 µl of concentrated hLPL complexed with GPIHBP1 and a Fab-fragment from the 5D2 antibody was injected onto a Superdex 200 Increase (5/150) column (GE Healthcare) equilibrated in 10 mM Tris, 150 mM NaCl, 10% (v/v) glycerol, 0.05% (w/v) CHAPS (0.8 mM), pH 7.2. Samples were exposed to X-rays while flowing at 0.2 ml/min through a temperature-controlled capillary (1.2 mm I.D.) at 20°C. During sample elution, we collected frames of 1.0 s exposure time. The sample-to-detector distance was 2.7 m covering a range of momentum transfer and 0.008 Å^{-1} ≤ s ≥ 0.6 Å^{-1} ($s = 4\pi\sin\theta/\lambda$, where 2θ is the scattering angle, and λ= 1.24 Å is the X-ray wavelength). Data from the detector were normalized to the transmitted beam intensity, averaged, placed on absolute scale relative to water and the scattering of buffer solutions subtracted using CHROMIXS (3).

All data manipulations were performed with PRIMUS*qt* and the ATSAS software package (4). The forward scattering *I(0)* and radius of gyration, R_g were determined from Guinier analysis (5) assuming that at very small angles ($s \leq 1.3/R_g$) the intensity is represented as $I(s)=I(0)\exp(-(sR_g)^{2/3})$. These parameters were also estimated from the full scattering curves using the indirect Fourier transform method implemented in the program GNOM (6), along with the distance distribution function *p(r)* and the maximum particle dimensions D_{max}. Molecular masses (*MMs*) of solutes were estimated from *I(0)* by computation of partial specific volume and the contrast between the glycosylated protein and the chemical components of the solution using the SASSIE server (http://sassie-web.chem.utk.edu/sassie2/). Theoretical scattering intensities were calculated using the program CRYSO (7).

Ab initio shape determination. Low resolution molecular shapes were reconstructed from SAXS data using the programs DAMMIF (8), which represents the macromolecule as a densely packed interconnected configuration of beads or chain-like ensemble of dummy residues, respectively, that best fits the experimental data $I_{exp}(s)$ by minimizing the discrepancy:

$$\chi^2 = \frac{1}{N-1}\sum_j \left[\frac{I_{\exp}(s_j) - cI_{calc}(s_j)}{\sigma(s_j)}\right]^2$$

where N is the number of experimental points, c is a scaling factor and $I_{calc}(s_j)$ and $\sigma(s_j)$ are the calculated intensity and the experimental error at the momentum transfer s_j, respectively. Multiple modeling runs were conducted to verify the stability of the solution, and to establish the most typical 3D reconstructions according to a spatial discrepancy measure using DAMAVER (9).

Hybrid Rigid body modeling. Rigid body models were computed from the experimental data using CORAL (10) and the available high-resolution structures of GPIHBP1•LPL (PDB 6E7K) and a representative monoclonal antibody fragment (PDB 1FGN) as rigid bodies. Glycosylation was introduced into the models based on mass spectrometry data using the GLYCOSYLATION routine of ATSAS (4) with a single $C_{40}N_2O_{29}H_{67}$ glycan attached to GPIHBP1 (Asn^{58}) and two $C_{68}N_4O_{49}H_{113}$ glycans attached to hLPL (Asn^{43} & Asn^{359}). Ambiguous distance restraints were employed for the GPIHBP1•LPL•5D2 structure calculations, with a 15 Å average distance between residues Asp^{28}, Lys^{30}, Gly^{68}, Glu^{93} (light chain); Glu^{54}, Ser^{101} (heavy chain) of the antibody, and the tryptophan-rich motif loop residues encompassed by Tyr^{414} and Ser^{422} of LPL used. SAXS data are deposited at the SASBDB (www.sasbdb.org) with accession code: SASDHF4.

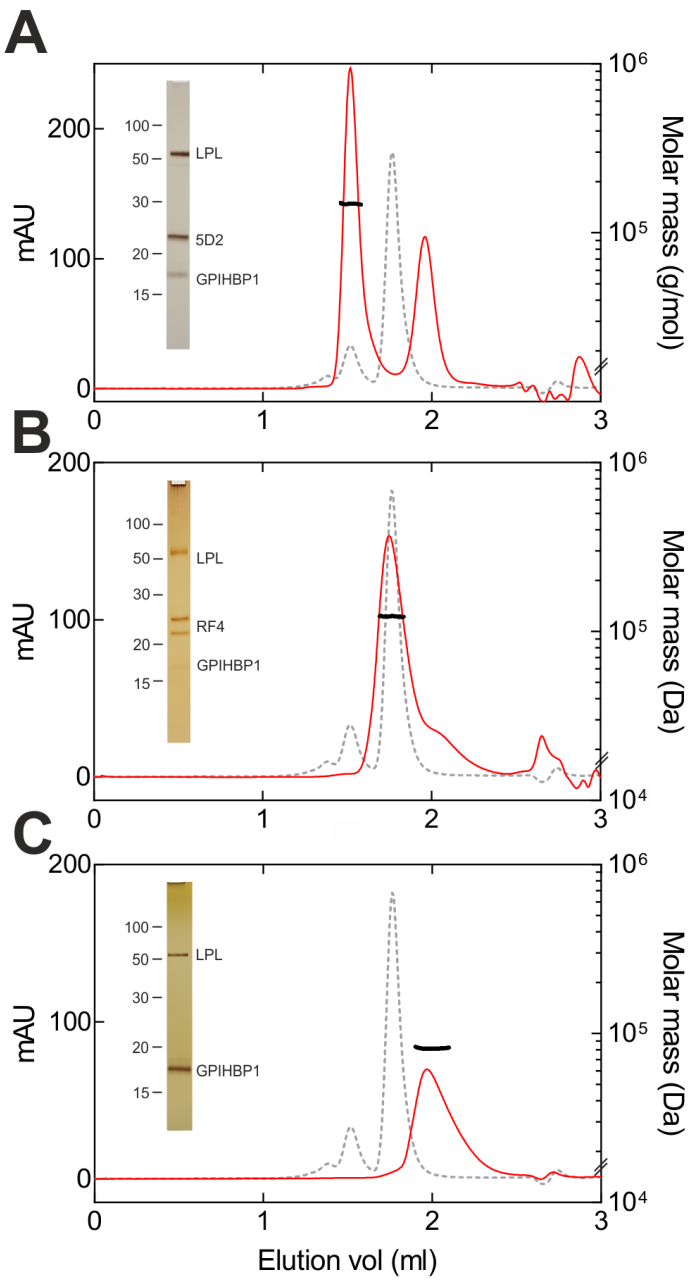

Fig. S1. Size-exclusion chromatography of hLPL complexes with multi-angle light scattering detection. *Panel A.* Elution of GPIHBP1•LPL•Fab-5D2 after size-exclusion chromatography on a Superdex200 Increase column in 10 mM Tris, 150 mM NaCl, 0.05% (w/v) CHAPS, 10% (v/v) glycerol, 0.05% (w/v) NaN_3, pH 7.2. *Panel B.* Elution of GPIHBP1•hLPL•Fab-RF4, note the late elution volume compared to the corresponding complex with Fab-5D2. *Panel C.* Elution of GPIHBP1•hLPL. The red lines show the absorbance profiles at 280 nm for the samples under investigation; the light gray hatched lines show the BSA control (monomer, dimer, trimer). The molecular masses determined using refractive indices as wells as scattering profiles are shown as solid black lines. The presence of all the various proteins (LPL, GPIHBP1, Fabs) in the eluting peak fractions were verified by SDS-PAGE of reduced and alkylated samples followed by silver staining (insets). Note, Fab-RF4 contains two polypeptides, which differ in their masses as confirmed by ESI-MS (see Fig. 3).

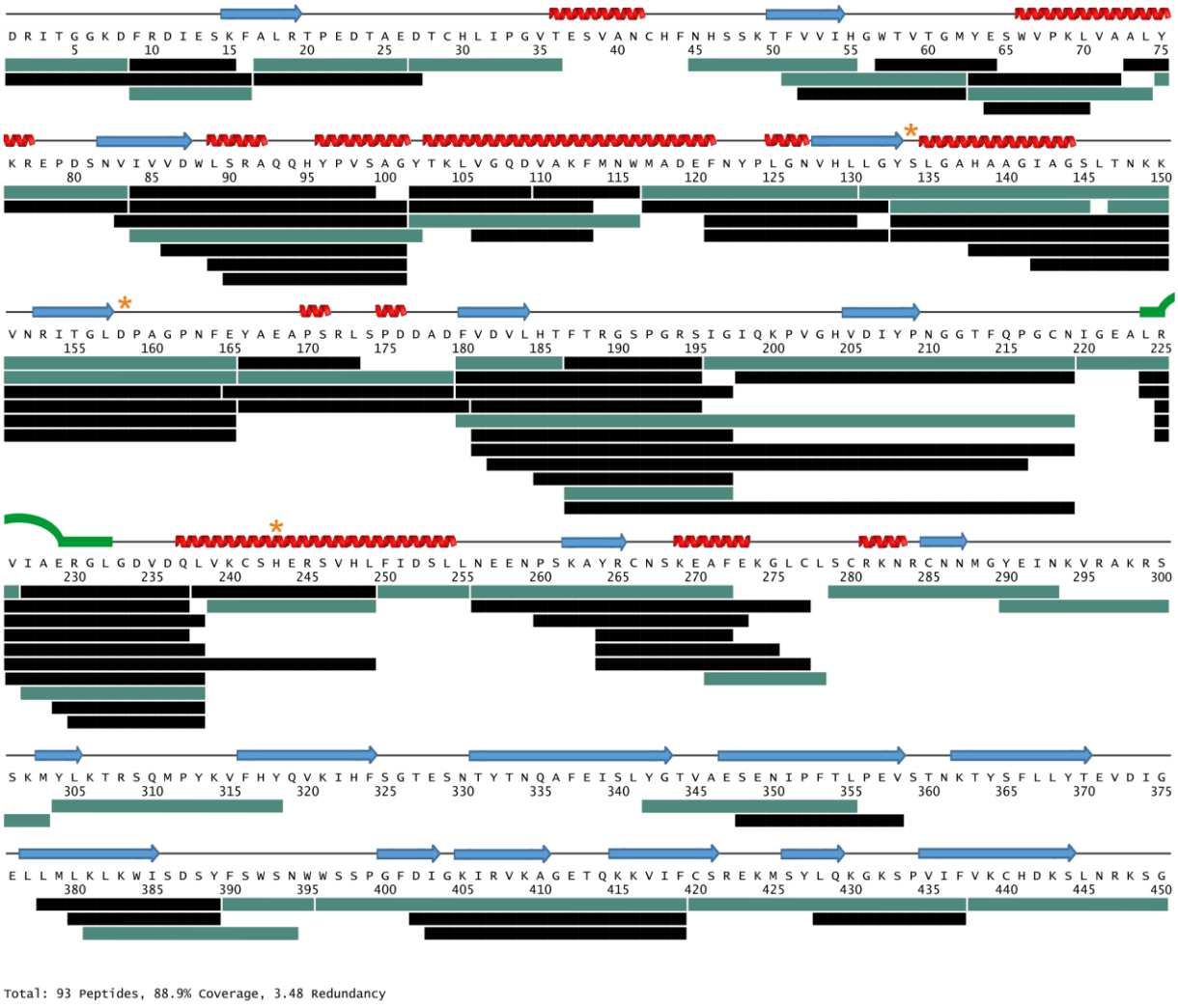

Fig. S2. A total of 93 peptic peptides were identified for bLPL, corresponding to an overall sequence coverage of 89%. The bars shown beneath the primary sequence of bLPL identify each of the 93 peptic peptides. The deuterium uptake values for peptides identified by the *green* bars are shown in *SI Appendix*, Fig. S3. Red helices and blue arrows above the primary sequence highlight secondary structure elements in LPL (α-helices and β-sheets, respectively). Orange asterisks show the catalytic triad residues, and the green loop indicates the position of the lid covering the active pocket.

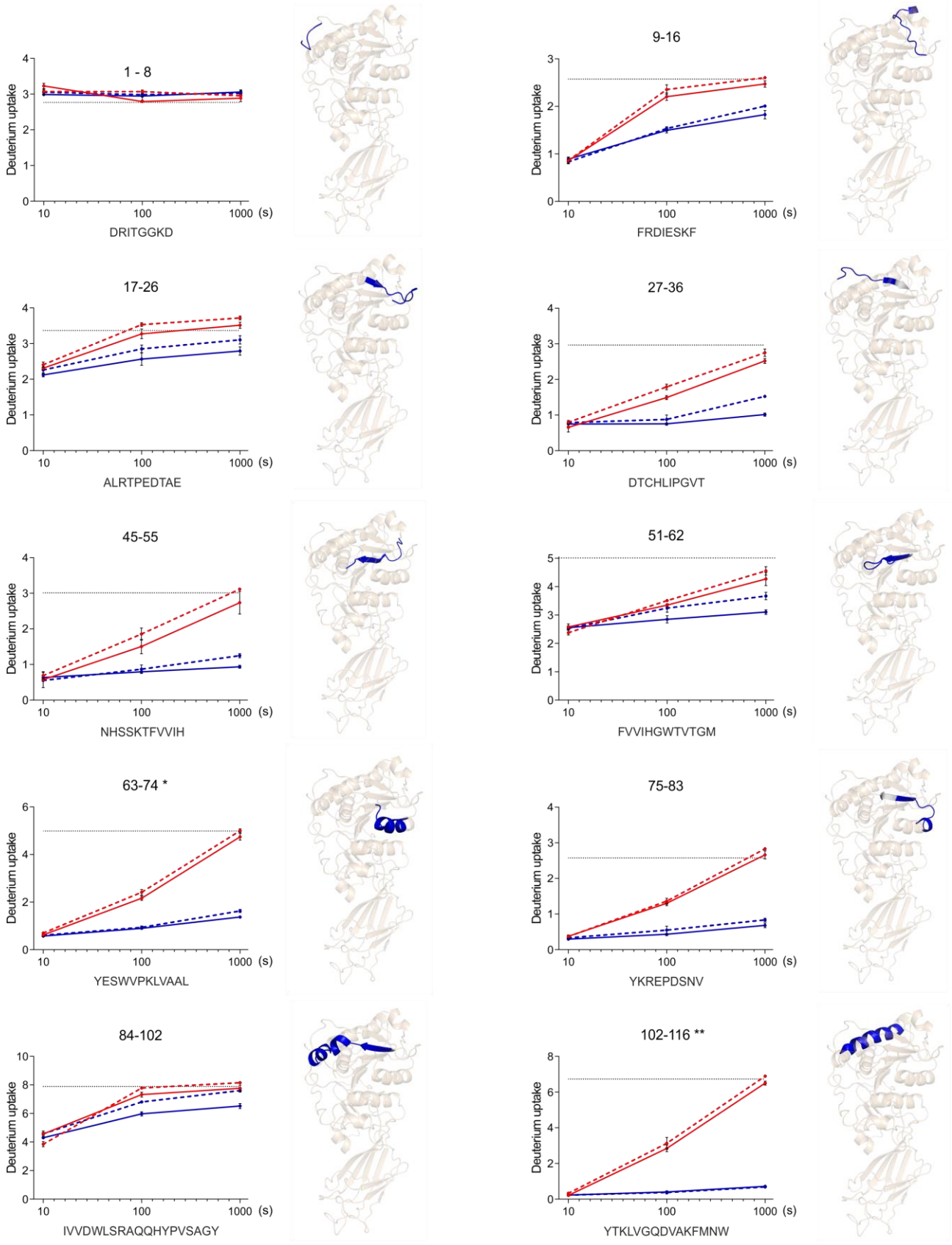
1 - 8
DRITGGKD
9-16
FRDIESKF
17-26
ALRTPEDTAE
27-36
DTCHLIPGVT
45-55
NHSSKTFVVIH
51-62
FVVIHGWTVTGM
63-74 *
YESWVPKLVAAL
75-83
YKREPDSNV
84-102
IVVDWLSRAQQHYPVSAGY
102-116 **
YTKLVGQDVAKFMNW
Deuterium uptake
(s)
LPL
LPL + Fab 5D2
LPL + GPIHBP1
LPL + Fab 5D2 + GPIHBP1

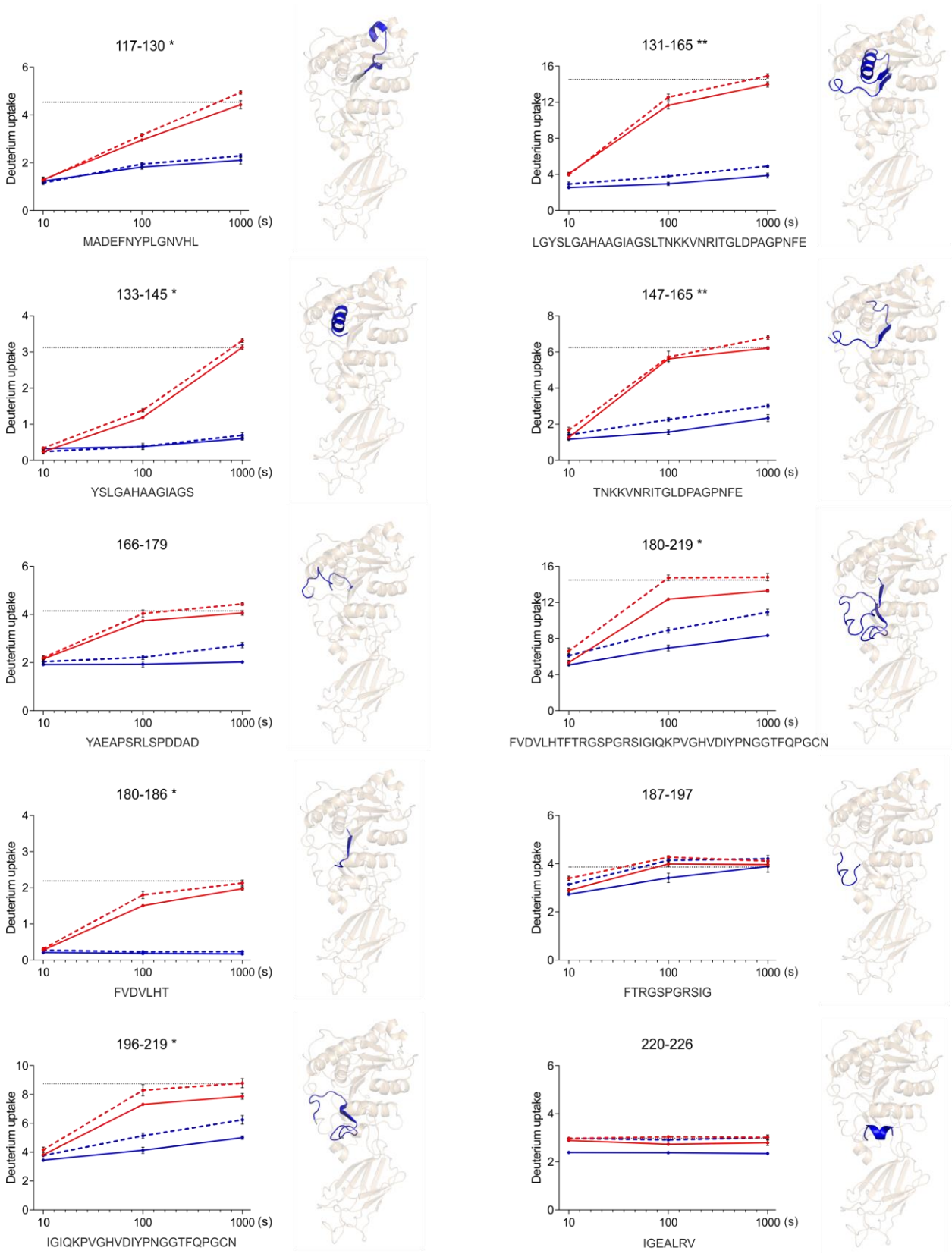
117-130 *
Deuterium uptake
MADEFNYPLGNVHL
131-165 **
LGYSLGAHAAGIAGSLTNKKVNRITGLDPAGPNFE
133-145 *
YSLGAHAAGIAGS
147-165 **
TNKKVNRITGLDPAGPNFE
166-179
YAEAPSRLSPDDAD
180-219 *
FVDVLHTFTRGSPGRSIGIQKPVGHVDIYPNGGTFQPGCN
180-186 *
FVDVLHT
187-197
FTRGSPGRSIG
196-219 *
IGIQKPVGHVDIYPNGGTFQPGCN
220-226
IGEALRV
10
100
1000 (s)
LPL
LPL + Fab 5D2
LPL + GPIHBP1
LPL + Fab 5D2 + GPIHBP1

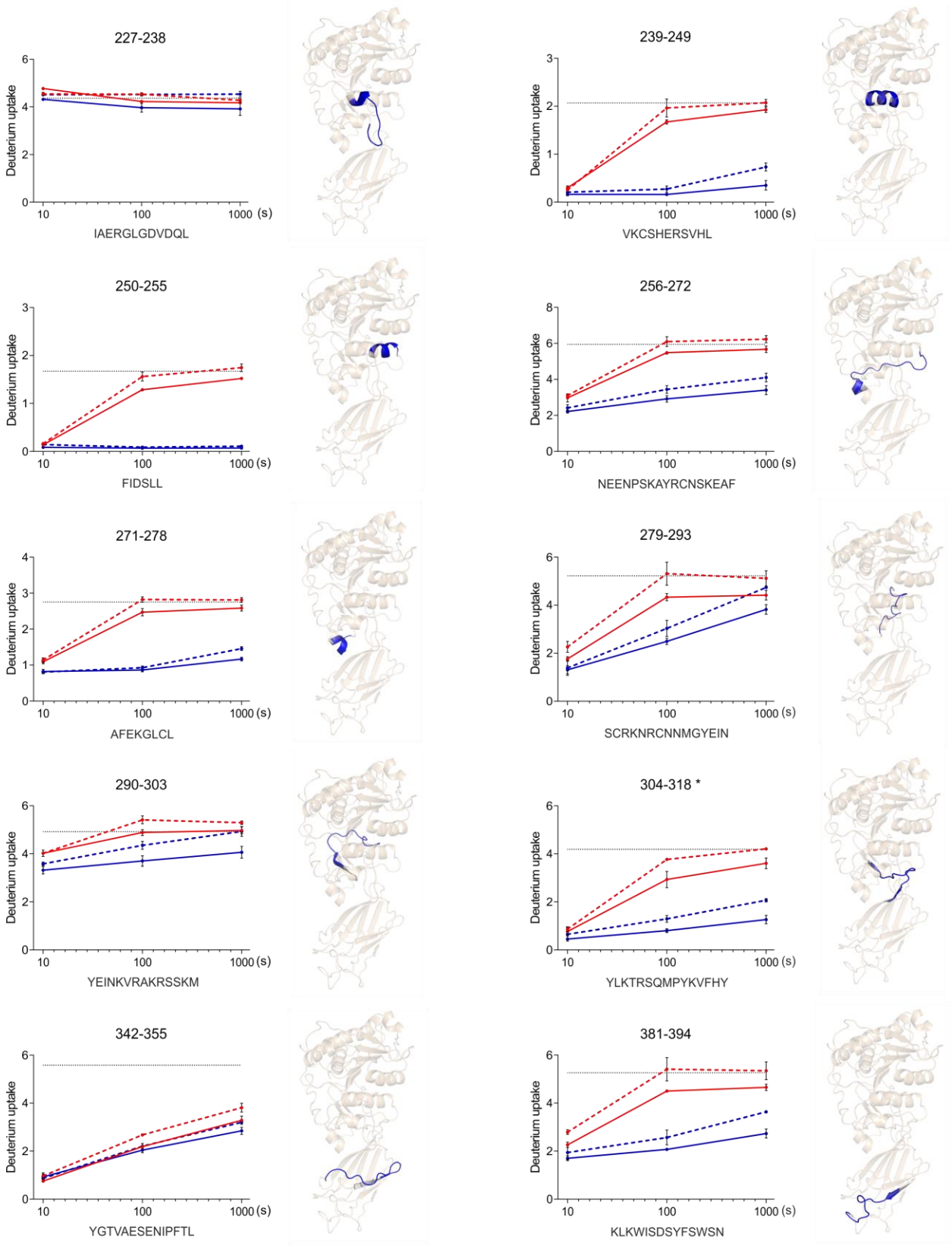
227-238
Deuterium uptake
IAERGLGDVDQL
239-249
VKCSHERSVHL
250-255
FIDSLL
256-272
NEENPSKAYRCNSKEAF
271-278
AFEKGLCL
279-293
SCRKNRCNNMGYEIN
290-303
YEINKVRAKRSSKM
304-318 *
YLKTRSQMPYKVFHY
342-355
YGTVAESENIPFTL
381-394
KLKWISDSYFSWSN
10
100
1000 (s)
LPL
LPL + Fab 5D2
LPL + GPIHBP1
LPL + Fab 5D2 + GPIHBP1

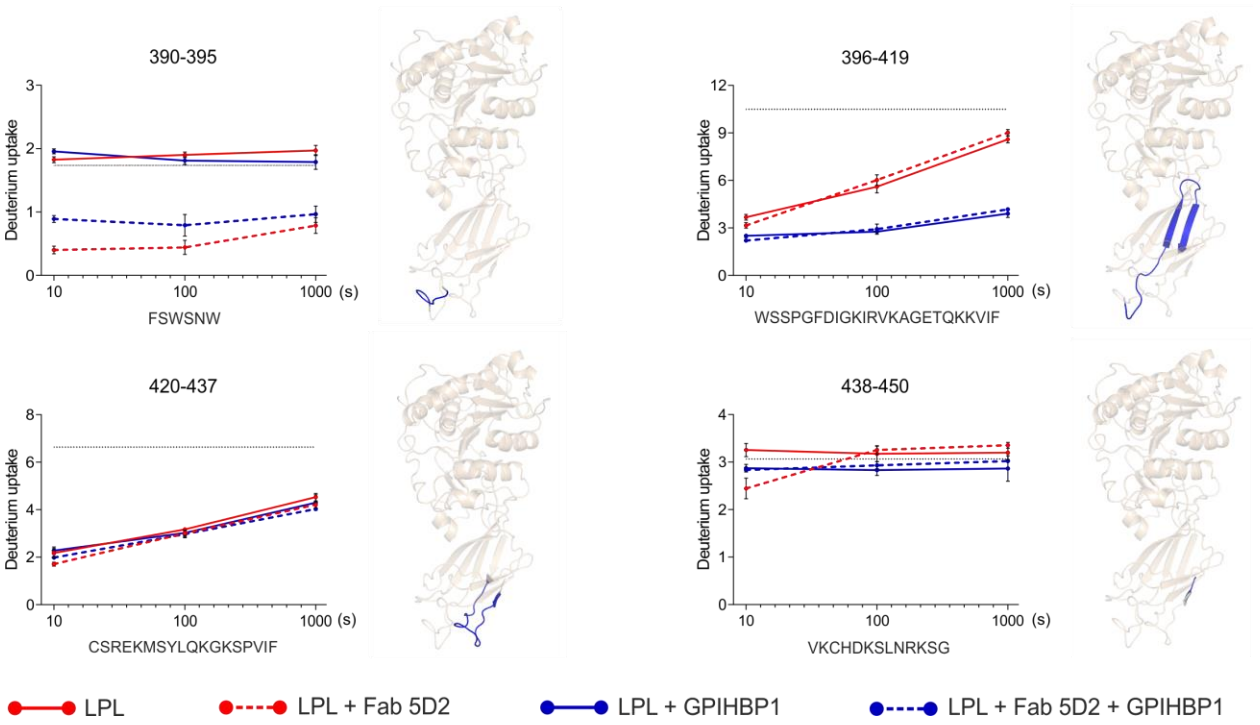

Fig. S3. Time-dependent deuterium uptake in bLPL alone and complexed with Fab-5D2 and/or GPIHBP1.These plots show the deuterium uptake in 43 peptic peptides covering the majority of LPL's primary sequence, both for LPL alone and LPL complexed with Fab-5D2 and/or GPIHBP1. The red lines show LPL; the blue lines show LPL•GPIHBP1 complexes, and the broken lines show the presence of Fab-5D2 in those samples. The position of the individual peptides in the LPL structure are highlighted by blue in the cartoon representation of LPL prepared with PyMol (Schrödinger) using the crystal structure of human LPL (PDB code 6OB0) (11) and their primary sequences are shown below the uptake plots. The deuterium content represent the average mass of the isotope envelopes and is shown as mean of three replicates with S.D. Signatures in the individual isotope envelopes suggesting correlated exchanges or coexisting conformations are marked by *(peak broadening) and **(bimodal isotope distribution).

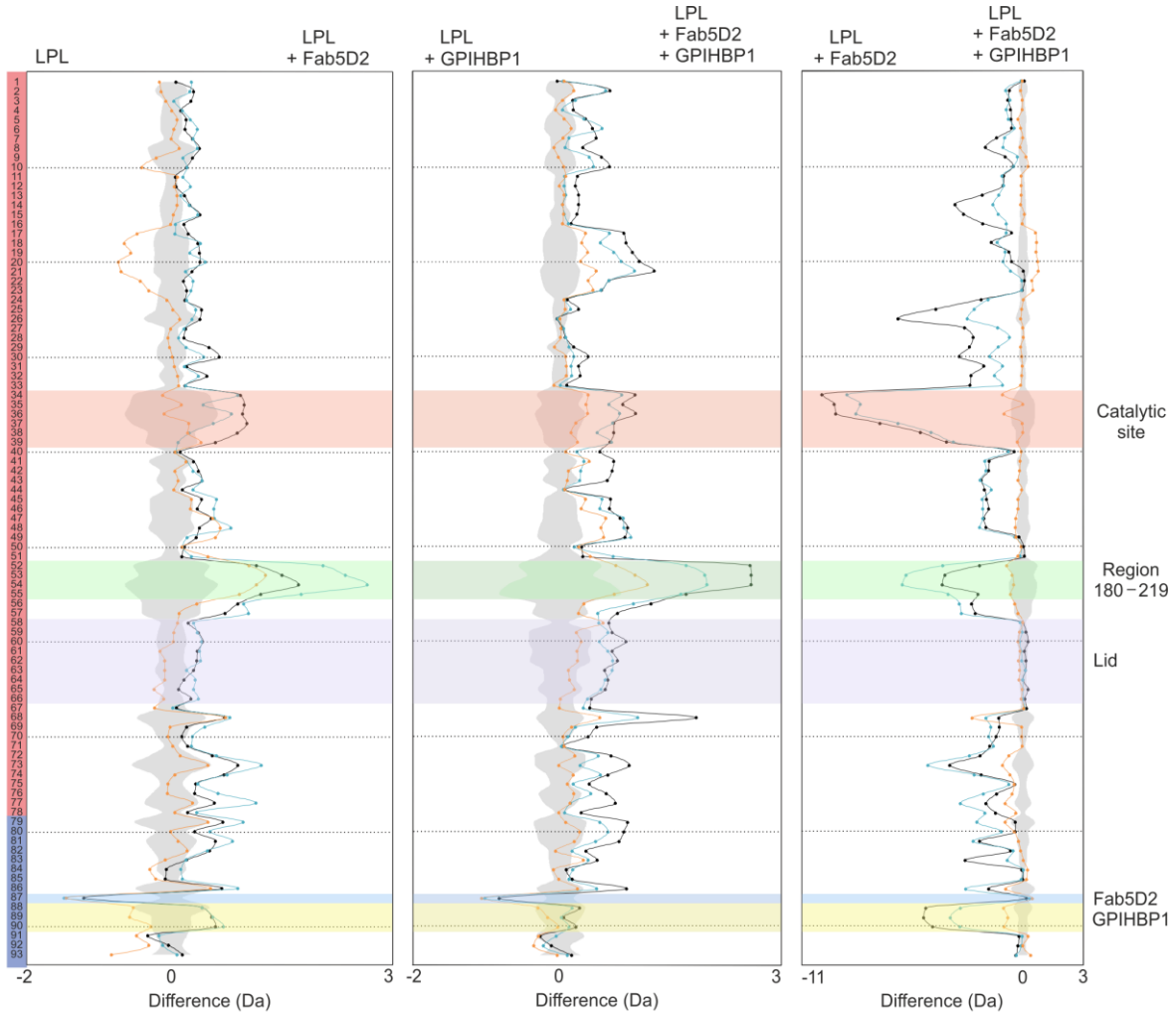

Peptide No.	Start	End	Sequence
1	1	8	DRITGGKD
2	1	16	DRITGGKDFRDIESKF
3	9	15	FRDIESK
4	9	16	FRDIESKF
5	17	26	ALRTPEDTAE
6	17	27	ALRTPEDTAED
7	27	36	DTCHLIPGVT
8	45	55	NHSSKTFVVIH
9	51	62	FVVIHGWTVTGM
10	52	62	VVIHGWTVTGM
11	57	64	YESWVPKL
12	63	72	YESWVPKLVA
13	63	74	YESWVPKLVAAL
14	64	70	ESWVPKL
15	73	83	ALYKREPDSNV
16	75	83	YKREPDSNV
17	83	101	VIVVDWLSRAQQHYPVSAG
18	84	99	IVVDWLSRAQQHYPVS
19	84	101	IVVDWLSRAQQHYPVSAG
20	84	102	IVVDWLSRAQQHYPVSAGY
21	86	101	VDWLSRAQQHYPVSAG
22	89	101	LSRAQQHYPVSAG
23	90	101	SRAQQHYPVSAG
24	102	109	YTKLVGQD
25	102	113	YTKLVGQDVAKF
26	102	116	YTKLVGQDVAKFMNW
27	106	113	VGQDVAKF
28	110	116	VAKFMNW
29	117	130	MADEFNYPLGNVHL
30	117	132	MADEFNYPLGNVHLLG
31	121	130	FNYPLGNVHL
32	121	132	FNYPLGNVHLLG
33	133	145	YSLGAHAAGIAGS
34	131	165	LGYSLGAHAAGIAGSLTNKKVNRITGLDPAGPNFE
35	133	164	YSLGAHAAGIAGSLTNKKVNRITGLDPAGPNF
36	133	165	YSLGAHAAGIAGSLTNKKVNRITGLDPAGPNFE
37	138	165	HAAGIAGSLTNKKVNRITGLDPAGPNFE
38	142	165	IAGSLTNKKVNRITGLDPAGPNFE
39	147	165	TNKKVNRITGLDPAGPNFE
40	165	179	EYAEAPSRLSPDDAD
41	166	173	YAEAPSRL
42	166	179	YAEAPSRLSPDDAD
43	166	180	YAEAPSRLSPDDADF
44	180	186	FVDVLHT
45	180	195	FVDVLHTFTRGSPGRS
46	180	197	FVDVLHTFTRGSPGRSIG
47	180	219	FVDVLHTFTRGSPGRSIGIQKPVGHVDIYPNGGTFQPGCN
48	181	195	VDVLHTFTRGSPGRS
49	181	197	VDVLHTFTRGSPGRSIG
50	181	219	VDVLHTFTRGSPGRSIGIQKPVGHVDIYPNGGTFQPGCN
51	182	216	HTFTRGSPGRSIGIQKPVGHVDIYPNGGTFQPGCN
52	185	197	HTFTRGSPGRSIG
53	187	195	FTRGSPGRS
54	187	197	FTRGSPGRSIG
55	187	219	FTRGSPGRSIGIQKPVGHVDIYPNGGTFQPGCN
56	196	219	IGIQKPVGHVDIYPNGGTFQPGCN
57	198	219	IQKPVGHVDIYPNGGTFQPGCN
58	220	226	IGEALRV
59	224	237	LRVIAERGLGDVDQ
60	224	238	LRVIAERGLGDVDQL
61	225	237	RVIAERGLGDVDQ
62	225	238	RVIAERGLGDVDQL
63	225	249	RVIAERGLGDVDQLVKCSHERSVHL
64	226	238	VIAERGLGDVDQL
65	227	237	IAERGLGDVDQ
66	227	238	IAERGLGDVDQL
67	229	238	ERGLGDVDQL
68	230	238	RGLGDVDQL
69	238	249	LVKCSHERSVHL
70	239	249	VKCSHERSVHL
71	250	255	FIDSLL
72	256	272	NEENPSKAYRCNSKEAF
73	256	277	NEENPSKAYRCNSKEAFEKGLC
74	260	273	PSKAYRCNSKEAFE
75	264	272	YRCNSKEAF
76	264	275	YRCNSKEAFEKG
77	264	277	YRCNSKEAFEKGLC
78	271	278	AFEKGLCL
79	279	293	SCRKNRCNNMGYEIN
80	290	303	YEINKVRAKRSSKM
81	304	318	YLKTRSQMPYKVFHY
82	342	355	YGTVAESENIPFTL
83	348	358	SENIPFTLPEV
84	378	389	LMLKLKWISDSY
85	380	389	LKLKWISDSY
86	381	394	KLKWISDSYFSWSN
87	390	395	FSWSNW
88	396	419	WSSPGFDIGKIRVKAGETQKKVIF
89	402	419	DIGKIRVKAGETQKKVIF
90	403	419	IGKIRVKAGETQKKVIF
91	420	437	CSREKMSYLQKGKSPVIF
92	428	437	LQKGKSPVIF
93	438	450	VKCHDKSLNRKSG

Fig. S4. Comparison of deuterium uptake in all peptic peptides recovered from LPL in different complexes with butterfly plots. These plots compare the differences in deuterium uptake for all peptic peptides recovered from bLPL in the different states: LPL *versus* LPL•Fab-5D2 (*panel A*); LPL•GPIHBP1 *versus* LPL•GPIHBP1•Fab-5D2 (*panel B*); and LPL•Fab-5D2 *versus* LPL•GPIHBP1•Fab-5D2 (*panel C*). In the case of bimodal peaks, deuterium uptake represent the average mass of both isotope envelopes and is the mean of three replicates. The shaded gray area corresponds to the largest standard deviation in the data sets recorded for each peptide (in triplicates). Transparent red and cyan colors on the left assign peptides to LPL's N-terminal hydrolase domain (NTD) or its C-terminal lipid-binding domain (CTD), respectively. The color shaded areas in the graphs highlight peptides covering the catalytic triad (red), the region 180–219 just before the lid (green), the lid (blue), the Fab-5D2 binding epitope (blue), and the GPIHBP1 binding epitope (yellow).The identity of the 93 unique peptic peptides recovered from LPL are shown in the bottom.

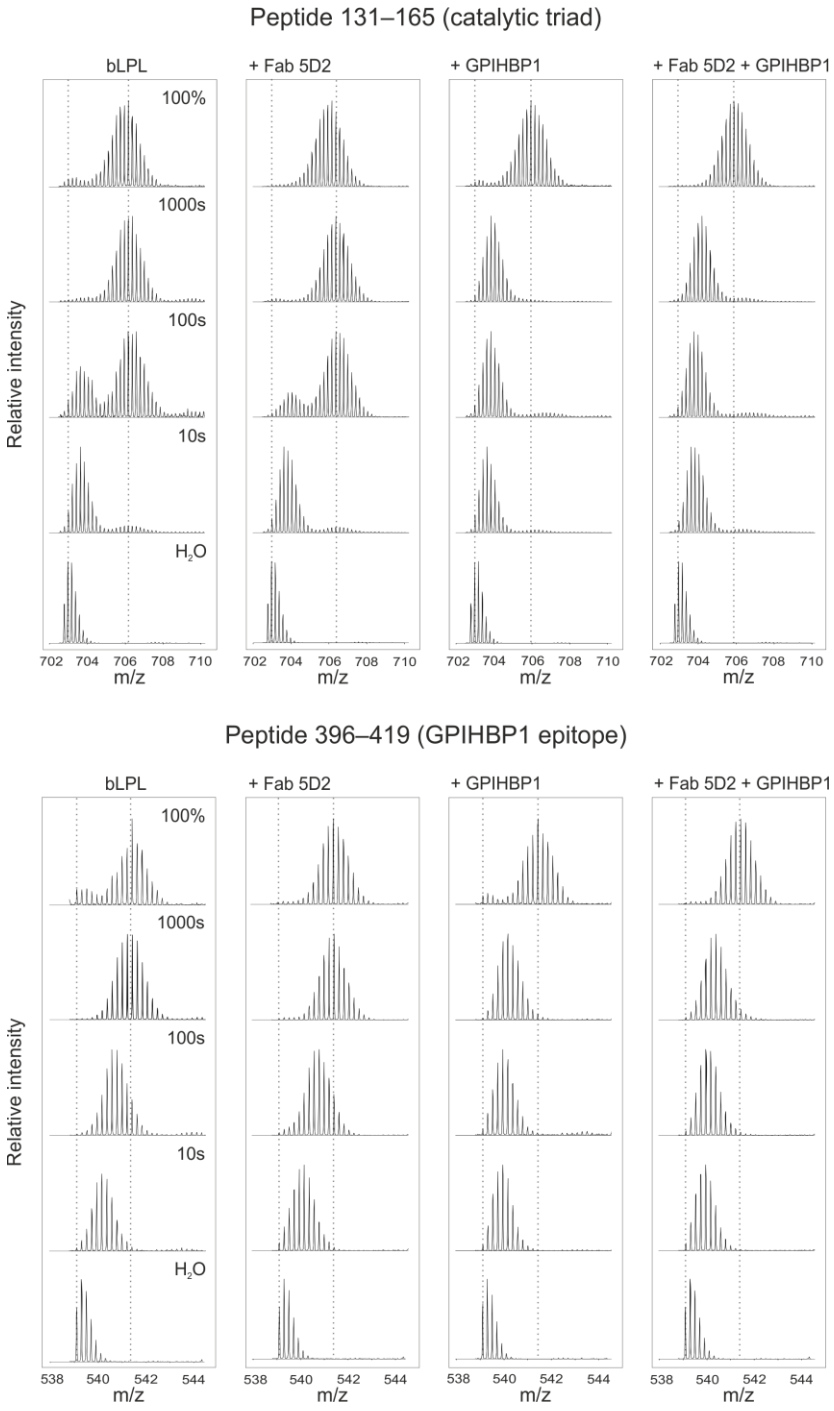

Fig. S5. Isotope envelopes revealing correlated and uncorrelated deuterium uptake in two different regions of LPL. The upper panel shows the temporal incorporation of deuterium into a region of LPL harboring the catalytic triad (residues 131−165). This region exhibits correlated exchange kinetics (resembling that of EX1), which signifies the progressive accumulation of protein populations with long-lived solvent exposure of that region (12). Binding GPIHBP1, but not Fab-5D2, prevents this slow transition. The lower panel shows a region of LPL exhibiting uncorrelated deuterium exchange (resembling EX2 kinetics) and binding of GPIHBP1 slows the rate of this exchange (residues 396−419).

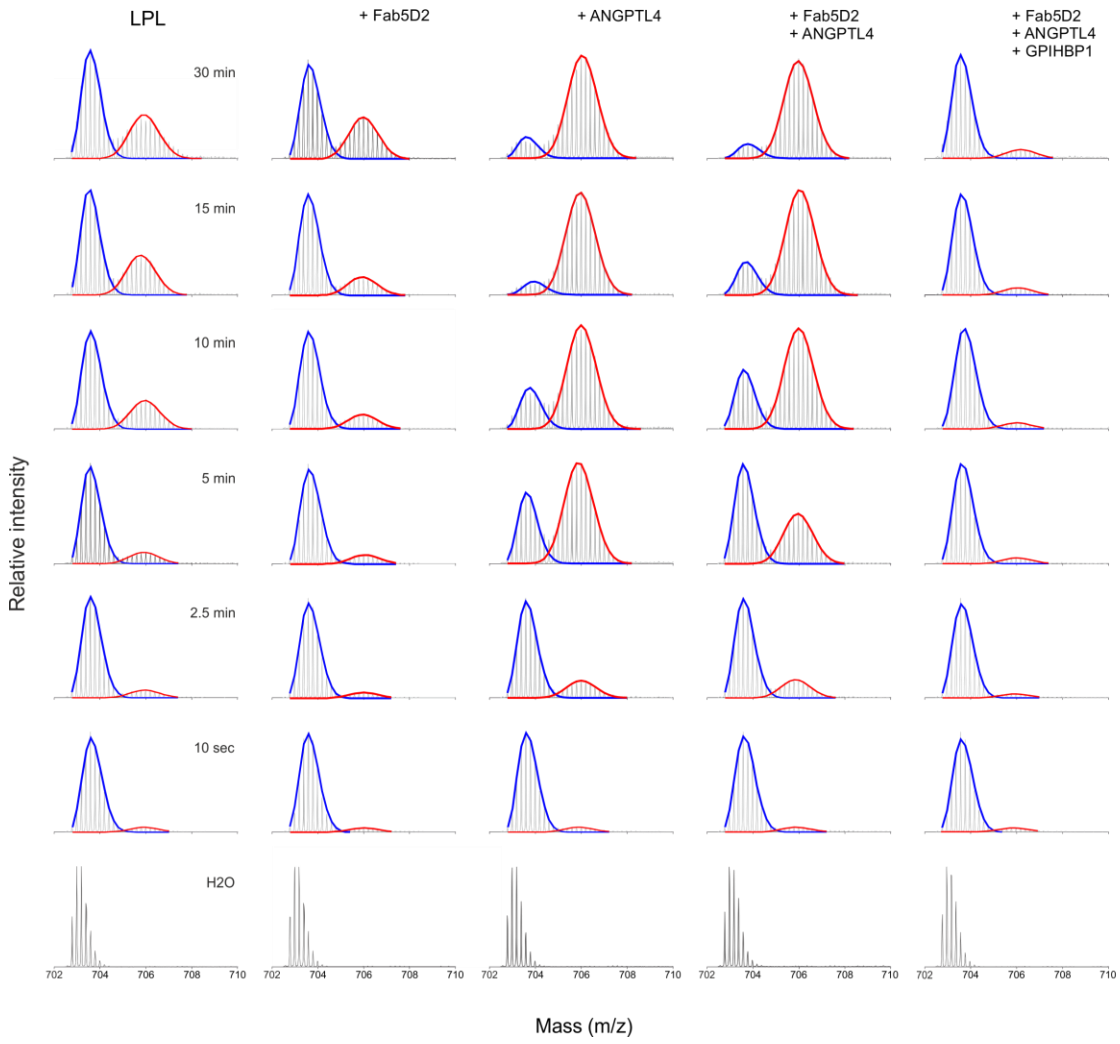

Fig. S6. Quantification of bimodal deuterium uptake in LPL by pulse labelling in deuterium oxide–containing buffers. The coexistence of folded and unfolded LPL in the absence and presence of sub-stoichiometric amounts of ANGPTL4 was measured by pulse-labeled HDX-MS. Shown are the isotope envelopes for a region of LPL harboring two of the three residues within the catalytic triad (residues 131−165). The progressive emergence of bimodality was quantified with the program HX-Express2 (13). The fractions of coexisting conformations in LPL are estimated by fitting two Gaussian distributions [folded state with low deuterium uptake (*blue line*) versus unfolded state with high deuterium uptake (*red line*)].

Table S1. Small-angle X-ray scattering data for Fab-5D2•LPL•GPIHBP1

(*a*) Sample details*	
	Fab-5D2•LPL•GPIHBP1
Organism	*Homo sapiens*
Source	*Drosophila* S2 (GPIHBP1); CHO cells (LPL); Sp2 myeloma cells (5D2)
UniProt sequence ID (residues in construct)	P06858 (29−475); Q8IV16 (21−151)
Extinction coefficient ε (280 nm, 0.1% w/v)	1.322
Partial specific volume $\bar{\upsilon}$ ($cm^3\,g^{-1}$)	0.725
Mean solute and solvent scattering length densities and mean scattering contrast $\Delta\bar{\rho}$ ($\rho_{protein}$-$\rho_{solvent}$) ($10^{10}\,cm^{-2}$)	2.75 (12.43−9.68)
Molecular mass *M* from chemical composition (monomer/dimer) (Da)	116610/233224
SEC–SAXS column, 5 × 150 mm Superdex S200 Increase (GE LifeScience)	
Loading concentration (mg ml^{-1}) [A280nm]	3.4
Injection volume (ul)	50
Flow rate (ml min^{-1})	0.3
Average concentration in combined data frames (mg ml^{-1})	0.4
Solvent composition (solvent blanks taken from SEC flowthrough prior to elution of protein)	10 mM Tris pH 7.2, 150 mM NaCl, 10% glycerol, 0.05% CHAPS
(*b*) SAS data collection parameters	
Instrument/Data processing	EMBL P12 (PETRA-III, DESY, Hamburg) with Pilatus6M detector (2)
Wavelength (Å)	1.24
Beam geometry (size, sample-to-detector distance)	0.12 × 0.25 mm^2, 3.0 m
s-measurement range ($Å^{-1}$)	0.002−0.7
Absolute scaling method	Comparison with scattering from 1.2 mm pure H_2O
Basis for normalization to constant counts	To transmitted intensity by beam-stop counter
Method for monitoring radiation damage	Frame comparison
Exposure time, number of exposures	900 s (900 × 1.00 s)
Sample temperature (ºC)	10

(*c*) Software employed for SAS data reduction, analysis and interpretation

SAS data reduction	*I(s)* versus *s* using *RADAVER* (ATSAS 2.8.3) (10), solvent subtraction using *PRIMUSqt* (ATSAS 2.8.3) (10)
Calculation of ε from sequence	*ProtParam (14)*
Calculation of $\Delta\overline{\rho}$ and $\overline{\upsilon}$ values from chemical composition	*SASSIE web server* (http://sassie-web.chem.utk.edu/sassie2/)
Basic analyses: Guinier, *P*(*r*), scattering particle volume (V_P)	*PRIMUSqt* from ATSAS 2.8.3 (10)
Shape/bead modelling	DAMMIF (8) and DAMMIN (15) via ATSAS online (https://www.embl-hamburg.de/biosaxs/atsas-online/)
Atomic structure modelling	CRYSOL (7), CORAL (10)
Molecular graphics	PyMOL v2.3 MacOS 10.13.6

(*d*) Structural parameters

Guinier Analysis	Fab-5D2•LPL•GPIHBP1
$I(0)$ (cm^{-1})	0.023 ± 0.001
R_g (Å)	48.8 ± 0.1
q-range ($Å^{-1}$)	0.012−0.015
M_r from $I(0)$ (Da)	100300
P(r) analysis	Fab-5D2•LPL•GPIHBP1
$I(0)$ (cm^{-1})	0.023 ± 0.002
R_g (Å)	48.2 ± 0.1
d_{max} (Å)	175 ± 5
q-range ($Å^{-1}$)	0.016−0.284
χ^2 (total estimate from *GNOM*)	1.0 (0.37)
M_r from $I(0)$ (Da) (ratio to predicted value)	100300 (0.82)
Volume (V_P) ($Å^3$)	187506

(*e*) Shape modelling results

DAMMIF (default parameters, 10 calc.)	Fab-5D2•LPL•GPIHBP1
q-range for fitting ($Å^{-1}$)	0.007−0.280
Symmetry/anisotropy assumptions	P1, none
NSD (standard deviation)	1.41 (0.16)
χ^2 value/range	1.12−1.12
Constant adjustment to intensities	8.7
P value	0.28−0.28
M_r estimate as 0.5 × volume of models (Da)	116977
Model resolution from *SASRES* (Å)	47 ± 4

(*f*) Atomistic modelling	
	Fab-5D2•LPL•GPIHBP1
CORAL rigid body modeling	
Starting crystal structures	PDB: 1fgn, 6e7k
Flexible residues	21−61,145−150 (GPIHBP); 415−422, 471−475 (LPL)
Glycans added with *GLYCOSYLATION* *	$C_{40}N_2O_{29}H_{67}$ (GPIHBP1) + 2 × $C_{68}N_4O_{49}H_{113}$ (LPL)
q-range for fitting (Å)	0.012-0.50
Symmetry, anisometry assumptions	P1, none
χ^2, *CORMAP P* value	1.07, 0.19
(*g*) SASBDB IDs for data and models	
Fab-5D2•LPL•GPIHBP1	SASDHF4

* For X-ray contrast, molecular weight and partial specific volume calculation it was assumed that the scattering particle consists of Fab-5D2, LPL, and GPIHBP1 with the following glycosylation composition: one $C_{40}N_2O_{29}H_{67}$ (GPIHBP1) and two $C_{68}N_4O_{49}H_{113}$ (LPL).

References

1. Chang SF, Reich B, Brunzell JD, & Will H (1998) Detailed characterization of the binding site of the lipoprotein lipase-specific monoclonal antibody 5D2. *J Lipid Res* 39:2350-2359.
2. Blanchet CE, *et al.* (2015) Versatile sample environments and automation for biological solution X-ray scattering experiments at the P12 beamline (PETRA III, DESY). *J Appl Crystallogr* 48:431-443.
3. Panjkovich A & Svergun DI (2017) CHROMIXS: automatic and interactive analysis of chromatography-coupled small-angle X-ray scattering data. *Bioinformatics* 34:1944-1946.
4. Franke D, *et al.* (2017) ATSAS 2.8: a comprehensive data analysis suite for small-angle scattering from macromolecular solutions. *J Appl Crystallogr* 50:1212-1225.
5. Guinier A (1939) La diffraction des rayons X aux très petits angles : application à l'étude de phénomènes ultramicroscopiques. *Ann. Phys.* 11:161-237.
6. Semenyuk AV & Svergun DI (1991) GNOM–a program package for small-angle scattering data processing. *Journal of Applied Crystallography* 24:537-540.
7. Svergun DI, Barberato C, & Koch MHJ (1995) CRYSOL—a program to evaluate X-ray solution scattering of biological macromolecules from atomic coordinates. *J Appl Crystallogr* 28:768-773.
8. Franke D & Svergun DI (2009) DAMMIF, a program for rapid ab-initio shape determination in small-angle scattering. *J Appl Crystallogr* 42:342-346.
9. Volkov VV & Svergun DI (2003) Uniqueness of ab-initio shape determination in small-angle scattering. *J Appl Crystallogr* 36:860-864.
10. Petoukhov MV, *et al.* (2012) New developments in the ATSAS program package for small-angle scattering data analysis. *J Appl Crystallogr* 45:342-350.
11. Arora R, *et al.* (2019) Structure of lipoprotein lipase in complex with GPIHBP1. *Proc Natl Acad Sci USA* 116:10360-10365
12. Ferraro DM, Lazo N, & Robertson AD (2004) EX1 hydrogen exchange and protein folding. *Biochemistry* 43:587-594.
13. Guttman M, Weis DD, Engen JR, & Lee KK (2013) Analysis of overlapped and noisy hydrogen/deuterium exchange mass spectra. *J Am Soc Mass Spectrom* 24:1906-1912.
14. Gasteiger E, *et al.* (2005) Protein identification and analysis tools on the ExPASy server. *The Proteomics Protocols Handbook*:571-607.
15. Svergun DI (1999) Restoring low resolution structure of biological macromolecules from solution scattering using simulated annealing. *Biophys J* 76:2879-2886.